ADVANCED FUNCTIONAL MATERIALS
www.afm-journal.de

Synthetic Colonic Mucus Enables the Development of Modular Microbiome Organoids

*Michael A. Miller and Scott Medina**

The human colon is home to trillions of microorganisms that modulate gastrointestinal physiology. The understanding of how this gut ecosystem impacts human health, although evolving, is slowed by the lack of accessible tools suitable to studying complex host-mucus-microbe interactions. Here, a synthetic gel-like material capable of recapitulating the varied structural, mechanical, and biochemical profiles of native human colonic mucus is reported to develop compositionally simple microbiome screening platforms with utility in microbiology and drug discovery. The viscous fibrillar material is realized through templated assembly of a fluorine-rich amino acid at liquid-liquid interphases. The fluorine-assisted mucus surrogate (FAMS) can be decorated with mucins to serve as a habitat for microbial colonization and integrated with human colorectal cells to generate artificial mucosae, referred to as a microbiome organoid. Notably, FAMS are made with inexpensive and commercially available materials and can be generated using simple protocols and standard laboratory hardware. As a result, this platform can be broadly incorporated into various laboratory settings to advance probiotic research and inform in vivo approaches. If implemented into high throughput screening approaches, FAMS may represent a valuable tool to study compound metabolism and gut permeability, with an exemplary demonstration of this utility presented here.

1. Introduction

The human gastrointestinal (GI) tract is host to a microbiome community of trillions of bacteria, diversified by around a thousand unique species.[1,2] These commensal microbes play critical roles in nutrient metabolism, immune training, and prevention of opportunistic infections.[3,4] Imbalance in the GI bacterial consortium is now implicated in the pathophysiology of several human diseases, including inflammatory bowel disorders,[5] type 2 diabetes,[6] and certain cancers.[7] The gut microbiome also impacts distal systems, including the brain where neurologic processes are altered via communication through the gut-brain axis.[8,9] Yet, despite its link to human health, our understanding of the functional properties of the gut microbiome, and how gut ecology influences human physiology, remains incomplete.

This gap in knowledge is largely due to a lack of facile and accessible tools suitable to studying, and controllably manipulating, complex host-mucus-microbe interactions.[10] Although gnotobiotic mice remain the gold standard, these expensive models are inaccessible for many researchers and do not always faithfully replicate human disease. In addition, it remains difficult to carefully shape microbiome composition and control mucus composition in the in vivo environment.[11,12] Tractable ex vivo models of the GI microbiome therefore represent powerful tools to study host-microbiota interactions in a multiparametric fashion at the cellular and molecular level.

Toward this goal, the development of gastrointestinal organoids—in vitro models of human intestinal epithelium—have expanded opportunities to study disease and probe microbe-host interactions ex vivo.[13,14] While these are valuable additions to the modeling spectrum, 3D systems are expensive, require significant technical training, and can be limited by access to primary material, making them difficult to implement in high-throughput applications. Monolayer cultures can address these limitations but are currently unable to faithfully replicate the colonic mucus, which is composed of inner and outer mucus layers that possess varied structural morphologies and densities.

Here, we report a self-assembling gel that can be engineered to replicate the diverse mechanical, structural, and biochemical profiles of colonic mucus. The material is generated from the interfacial organization of a non-natural amino acid at fluorous-water interphases to form a viscous, double-layer, colloid of fibrillar and coacervate assemblies. We demonstrate this synthetic platform can be readily coated with a variety of mucin proteins and directly incorporated into multicellular systems to create customizable ex vivo microbiome organoids. We show that the mechanical, structural, and biochemical properties can be independently tailored to create designer multicellular systems

M. A. Miller, S. Medina
Department of Biomedical Engineering
Pennsylvania State University
University Park, PA 16802-4400, USA
E-mail: shm126@psu.edu
S. Medina
Huck Institutes of the Life Sciences
Pennsylvania State University
University Park, PA 16802-4400, USA

The ORCID identification number(s) for the author(s) of this article can be found under https://doi.org/10.1002/adfm.202402514

DOI: 10.1002/adfm.202402514

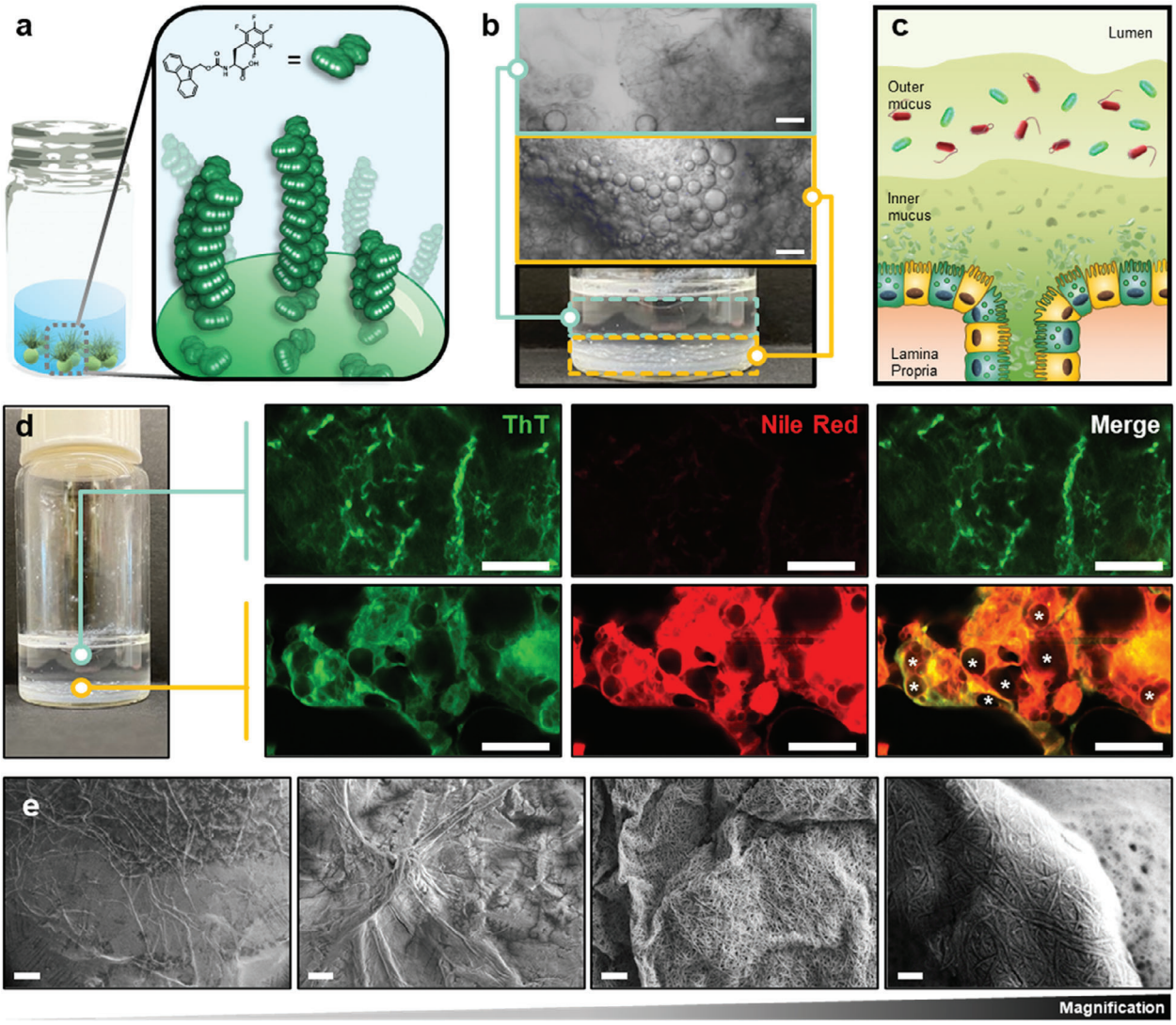

Figure 1. Development of double layer Fmoc-F_F fibrillar gels. a) Conceptual schematic of Fmoc-F_F assembly at fluorous-water interfaces to evolve percolating fibrils. b) Representative optical images and micrographs of Fmoc-F_F gels demonstrating the viscous PFD coacervate bottom layer (yellow) and fibrillar upper layer (teal). Scale bars = 200 µm. c) Schematic representation of human colonic double-layered mucus. d) Representative fluorescent micrographs of Fmoc-F_F:PFD structures in the upper (top) and lower (bottom) material layers. * indicate coacervate droplets. Scale bars = 50 µm. e) Representative scanning electron microscopy images of the Fmoc-F_F fibrillar gel upper layer, at varying magnification. Scale bars (from left to right) = 200, 20, 2, and 0.2 µm.

amenable to high throughput applications. As an exemplary demonstration, we incorporate these materials into a gastrointestinal permeability assay and demonstrate their ability to model oral bioavailability of macromolecular compounds.

2. Results and Discussion

2.1. Fabrication and Molecular Characterization of Synthetic Mucus

While screening a surfactant library to prepare fluorous emulsions we discovered the ability of the non-natural amino acid, Fmoc-pentafluoro-L-phenylalanine (Fmoc-F_F), to form viscous, mucus-like, gels at liquid-liquid phase separated interfaces (**Figure 1a**). The material is generated by pipetting a solution of perfluorodecalin (PFD) containing Fmoc-F_F (20 mmol L^{-1}) into saline, leading to the spontaneous supramolecular organization of the amino acid at the fluorous-water interface. This rapid and irreversible step produces a dense coacervate gel, from which a fibrillar network evolves into the aqueous fraction when incubated at 37 °C (Figure 1b). This double layered structure mimics the typical morphology of colonic mucus, which is characterized by a dense inner layer that adheres to epithelial cells and a diffuse fibrillar outer layer that harbors commensal bacteria (Figure 1c). To further visualize the bilayer composition of our synthetic mucus, the lipophilic dye Nile red was dissolved in the PFD solvent before gel fabrication. Thioflavin T (ThT), a dye that displays enhanced fluorescence upon binding to amyloid structures,[15]

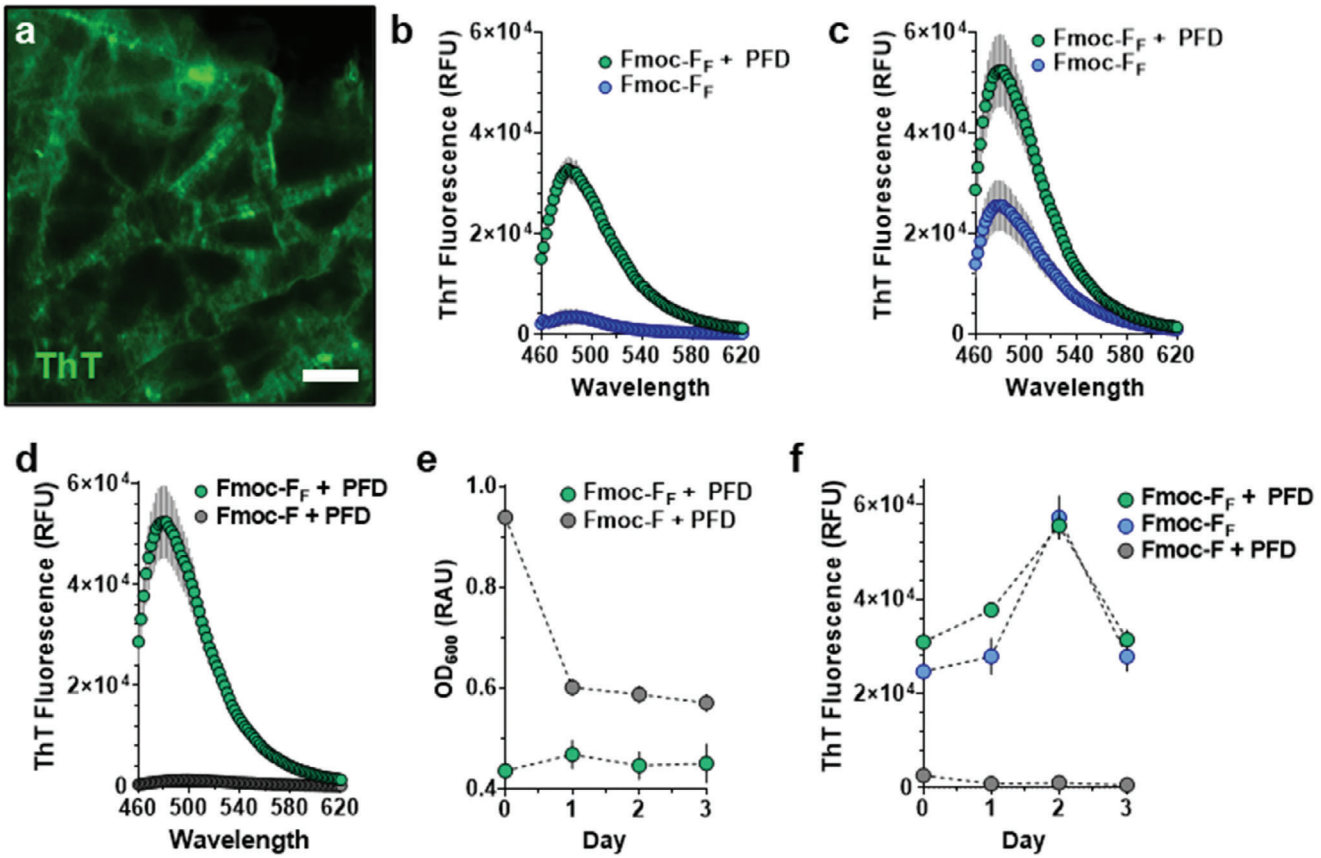

Figure 2. Mechanistic investigation of Fmoc-F_F assembly. a) Representative fluorescent micrograph of ThT-stained Fmoc-F_F fibrillar bundles. Scale bar = 40 µm. b,c) Average fluorescence spectra of ThT dye in the presence of Fmoc-F_F pre-dissolved in PFD before creating liquid-liquid phases in saline (green) or direct dissolution of Fmoc-F_F in saline alone (blue) at b) 1 and c) 2 days of incubation. RFU = Relative Fluorescence Units. d) Average fluorescence spectra of ThT dye in the presence of Fmoc-F_F (green) or non-fluorinated Fmoc-F (grey) amino acids assembled at PFD-saline interfaces after 2 days of incubation. e,f) Time-dependent optical density ((e) OD_{600}) and ThT fluorescence (f) profile of amino acid assemblies prepared under the indicated conditions. Data shown in panels (b–d) represents average ± s.e.m. of $n = 3$ replicates, with individual data points underlaid. Data shown in panels (e,f) represents average ± s.e.m. of $n = 63$, measured from $n = 3$ experimental replicates.

was added to the aqueous fraction to label Fmoc-F_F assembled fibrils. Representative fluorescent micrographs shown in Figure 1d demonstrate that the bottom layer of the material is a tightly packed network of PFD droplets, from which Fmoc-F_F assembly initiates at the fluorous-water interface. Co-localization of Nile red and ThT signals suggests these interfacial structures are amorphous hydrophobic oligomers and/or protofibrils, representing the nascent stages of Fmoc-F_F assembly. Conversely, the upper layer is a diffuse collection of extended fibers characterized only by ThT fluorescence, with a marked absence of Nile red (Figure 1d, top). This suggests these are mature, organized fibrils that have evolved from rearrangement of the disorganized structures templated in the lower coacervate layer. Parallel electron microscopy, shown in Figure 1e, further demonstrates that the less dense upper layer is an interpenetrating system of Fmoc-F_F self-assembled fibrils. The cohesivity of this layer is imparted via non-covalent entanglement of fibers, creating a porous mesh-like architecture.

Next, we investigated the nature and rate of molecular organization of Fmoc-F_F assemblies using the ThT dye. The multilamellar appearance of ThT-stained fibers suggests they are composed of β-sheet like plates that organize through n→π^* stacking of Fmoc-F_F residues (**Figure 2a**).[16,17] This organization is strongly induced by the presence of the phase-separated PFD droplets, as demonstrated by the attenuated ability of Fmoc-F_F to form fibers when PFD is absent in the saline solution (Figure 2b). Here, the PFD-aqueous interface serves to rapidly template the assembly of Fmoc-F_F monomers into a stable gel, from which fibers continue to grow and evolve over several days (Figure 2c).

To further investigate this assertion, and specifically isolate fluorine–fluorine driven effects, we evaluated the assembly of non-fluorinated Fmoc-L-phenylalanine (Fmoc-F) under similar conditions (Figure 2d). Results show this fluorine-deficient analog is not capable of forming viscous fibrillar gels and instead generates colloidal emulsions, as indicated by the combination of high optical density (Figure 2e) and low ThT fluorescence (Figure 2f). Prior studies from our group suggest these divergent assembly pathways result from the propensity for perfluorocarbon-water systems to preferentially direct J-aggregate formation of Fmoc-F_F, and not the non-fluorinated Fmoc-F analog.[17] This leads to Fmoc-F_F being uniquely organized into anti-parallel arrangements, where fluorenyl

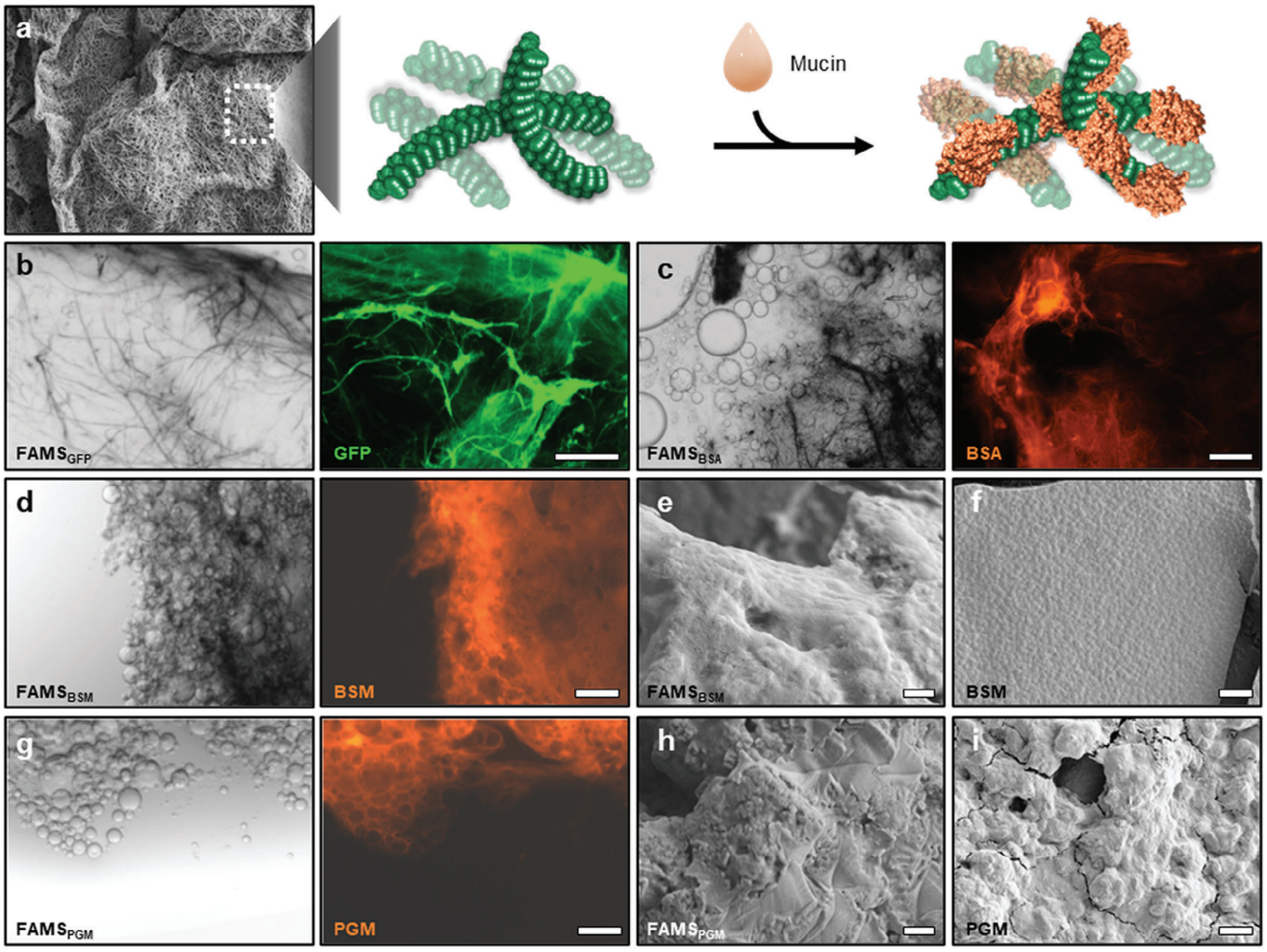

Figure 3. Protein-coating of FAMS gels. a) Schematic representation of non-covalent mucin coating of the FAMS fibrillar surface (SEM micrograph reused from Figure 1e). b,c) Representative Optical (left) and fluorescent (right) micrographs of GFP (b) and Cy5-labeled BSA (c) coated FAMS. Scale bars = 200 µm. d–i) Representative optical (left) and fluorescent (right) micrographs of Cy5-labeled bovine submaxillary mucin ((d) BSM) and porcine gastric mucin ((g) PGM) coated FAMS. Associated scanning electron microscopy images of FAMS surface after e) BSM or h) PGM coating. SEM images of native f) BSM and i) PGM reconstituted mucin gels shown for comparison. Scale bars in panels (d) and (g) = 200 µm. Scale bars in remaining panels = 1 µm.

moieties form alternate β-sheets to create π-stacked pairs with interleaved fluorinated phenyl rings. Propagation of these stacked assemblies likely yields the observed fibrils.[17] Persistence of these structures for over a year, as indicated by optical density measurements, suggests the fibrillar arrangements represent a thermodynamic assembly minimum (Figure S1, Supporting Information). However, a sharp drop in ThT fluorescence after two weeks of incubation indicates the intrafibrillar arrangement of Fmoc-F_F units continues to evolve after initial organization (Figure S1, Supporting Information). Given the unique hierarchical organization of Fmoc-F_F, induced by the presence of the perfluorinated phenyl ring and perfluorocarbon droplet interface, we hereafter refer to the assembled material as fluorine-assisted mucus surrogate, or FAMS.

To prepare the surface of FAMS for bacterial attachment we next coated the fibrils with mucin proteins (**Figure 3a**). Here, simple addition of a protein solution to pre-formed FAMS led to rapid and robust fibril adsorption, producing a protein surface coating that was stable to multiple washes with media. Optimization of the coating procedure was done using two model fluorescent proteins, GFP and Cy5-BSA. Fluorescence microscopy demonstrated these proteins non-covalently decorate the materials and are retained after multiple washings (Figure 3b,c). Similar studies were then performed using Cy5-labeled bovine submaxillary mucin (BSM) and porcine gastric mucin (PGM). As expected, addition of BSM lead to uniform coating of the material network (Figure 3d), with additional SEM imaging demonstrating a relatively smooth surface topography to BSM-coated FAMS (FAMS$_{BSM}$, Figure 3e). This resembled the topology of reconstituted mucus prepared from the BSM protein stock (Figure 3f), suggesting the mucin assembles into cohesive sheets that envelop the FAMS fibrillar network. Coating with PGM was similarly successful (Figure 3g), although the surface morphology was more irregular (Figure 3h) due to the uneven assembly of PGM itself (Figure 3i). SEM imaging confirmed the morphology

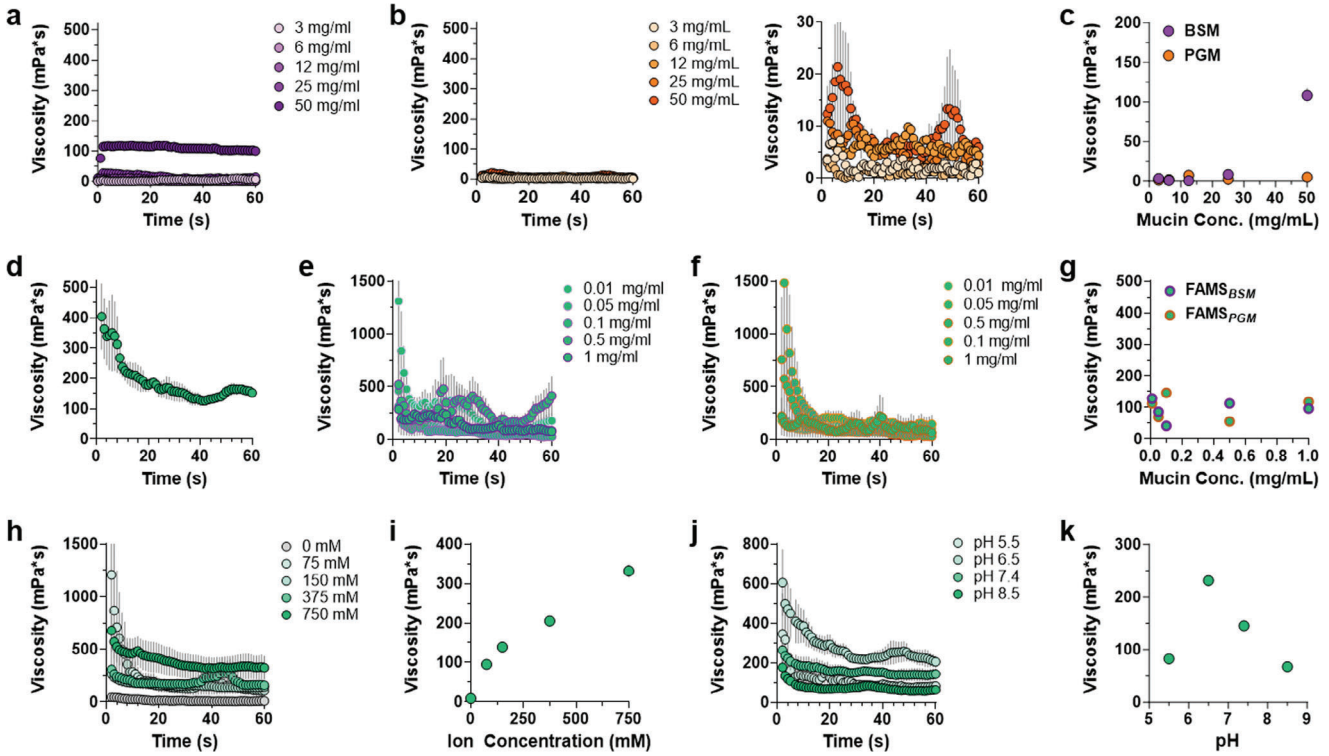

Figure 4. Rheological characterization of FAMS. a,b) Time- and concentration-dependent dynamic viscosity curves for a) BSM or b) PGM reconstituted gels. Panel b, left, shows the viscosity profile of PGM at a matched *y*-axis scale to panel a for comparison. Panel b, right, shows a reduced *y*-axis scale to better visualize curves. c) Concentration-dependent equilibrium viscosity for BSM (purple) or PGM (orange) reconstituted gels. d) Time-dependent dynamic viscosity profile of FAMS gels. e,f) Time-dependent dynamic viscosity of FAMS gels coated with varying concentrations of e) BSM or f) PGM. g) Concentration-dependent equilibrium viscosity for FAMS gels coated with BSM ($FAMS_{BSM}$) or PGM ($FAMS_{PGM}$). h,j) Time-dependent dynamic viscosity of uncoated FAMS gels in phosphate buffered saline at varying salt concentration (h) or pH (j). i,k) Concentration-dependent equilibrium viscosity for uncoated FAMS gels as a function of ion concentration ((i) $n \geq 72$) or pH ((k) $n = 90$). Data shown represents average ± s.e.m. of $n = 3$, unless otherwise stated. All measures taken from n = 3 experimental replicates for each time point. Replicas of panels a–f, h, and j with all individual points shown can be found in Figure S5 (Supporting Information).

of BSM and PGM coatings were consistent across multiple length scales (Figures S2 and S3, Supporting Information). Reducing the BSM coating concentration to visualize the underlying fibrillar network demonstrated that the addition of mucins does not disrupt the integrity of the FAMS super-structure (Figure S4, Supporting Information). In sum, our results support the ability of FAMS to assemble into a mucin-rich double-layer material that approximates the structural and biochemical characteristics of colonic mucus.

2.2. Mechanical Analysis of Mucin-Functionalized FAMS

A key checkpoint for mimicry of GI colonic mucus is material viscoelasticity, as the ability of native mucus to flow over long loading periods is necessary for the movement of solids during peristalsis. Mucus viscosity also has important implications in shaping microbial behavior and contributes to disease. For example, *H. pylori* alters environmental pH to reduce the viscoelasticity of gastric mucus, thereby compromising the integrity of its barrier function.[18] Similarly, several intestinal microbial pathogens secret proteases that degrade MUC2 to modulate mucus viscosity during pathogenesis,[19] leading to pro-inflammatory contact between gut flora and immune cells.[20]

Recent rheologic studies show healthy human colonic mucus is composed of 1.3–1.9 wt.% (13–19 mg mL^{-1}) mucin solids, yielding a dynamic viscosity of 150–250 mPa s.[21] Using this benchmark, our first mechanical characterization step was to assess the baseline viscosity for the mucins themselves when reconstituted in saline (**Figure** 4a–c). Rheological dynamic time sweep measurements of reconstituted BSM showed a dynamic viscosity of 1–114 mPa s as mucin concentration was increased from 3–50 mg mL^{-1}, resembling the rheological performance of native human colonic mucus.[21] PGM was less viscous, reaching an average dynamic viscosity of 6 mPa s at the highest tested concentration. We next tested the viscosity of native FAMS without mucin coating. Results in Figure 4d demonstrate a prolonged stress relaxation response of the viscoelastic material over the first 40 s of loading, reaching a plateau dynamic viscosity of ≈150 mPa s. This behavior is similar to the long stress-relaxation response reported for porcine gastric mucus gels.[22] Mucus viscoelasticity results from reversible, non-covalent interactions between mucin components, enabling solid-like responses over short loading periods and flow behavior on longer time scales. Interestingly, while FAMS was able to replicate the viscoelastic

nature of native mucus, we did not observe this same flow behavior for reconstituted BSM and PGM (Figure 4a,b). This is likely due to the compositional simplicity of these solutions, which do not replicate the varied biomolecular constituents and gradient structural morphology of native GI mucus.

With these benchmarks established, we next tested the mechanical performance of FAMS coated with BSM (Figure 4e) and PGM (Figure 4f) mixtures. Rheological measurements demonstrate that, although the relaxation behavior of native FAMS is retained, the initial dynamic viscosity magnitude is greater when the gels are coated with mucins than without. Still, mucin-coated FAMS were found to maintain a ≈100 mPa s plateau regardless of the loaded mucin concentration (Figure 4g).

Given the sensitivity of GI mucus to changes in environmental ionic strength and pH, we next tested these parameters on the viscosity of FAMS. Increasing the total salt concentration of the phosphate buffered saline environment from 0–750 mM led to a corresponding increase in FAMS viscosity (Figure 4h,i). This is converse to native mucus, where increasing ion strength generally correlates to reduced viscosity due to polyelectrolyte charge-shielding.[23] In our case, screening of the Fmoc-F_F anionic charge by salt may alter its solubility and shift its kinetic equilibrium in favor of fibrillar assembly, thereby producing a more cohesive and viscous FAMS gel. Changing solution pH also led to variable FAMS viscoelastic responses (Figure 4k). Here, average dynamic viscosity increased from 83 mPa s at pH 5.5 to 231 mPa s at pH 6.5, before declining as the solution became more basic. This bears resemblance to native mucus, which exhibits decreasing viscosity as environmental pH transitions from neutral to weakly alkaline.[24] The ability of FAMS to mechanically respond to its environment is most likely regulated by the protonation state of Fmoc-F_F's carboxylic acid. This is supported by studies on various Fmoc-Phe derivatives demonstrating that changes in ionic strength and pH modulate Coulombic repulsion between anionic charged amino acids to alter their assembly propensities.[16,25] In sum, our results show that the viscoelastic behavior of FAMS can be modulated by environmental conditions to create mucus analogs with customizable rheologic properties that match native colonic mucus.

2.3. Development of Synthetic Microbiome Organoids

Microbial integration into FAMS was initially investigated using a stably expressing GFP-*E. coli* strain to aid visualization. Although *E. coli* was able to bind to the surface of uncoated FAMS, its attachment was relatively poor as indicated by low cellular fluorescence (**Figure 5**a). Conversely, mucin coatings led to significant *E. coli* colonization on, and within, the fibrillar scaffold, forming dense microbial communities (Figure 5b–d; Figure S6, Supporting Information). Scanning electron microscopy confirmed that the microbes did not simply reside at the surface of the material, but integrated within the fibrillar mesh (Figure 5e,f; Figure S7, Supporting Information).

Next, growth studies evaluated the proliferation of *E. coli* seeded onto the FAMS materials over a 24 h incubation period (Figure 5g). These assays were performed in sterile PBS to minimize environmental nutrients, and thereby allow us to isolate the effects of FAMS coatings on *E. coli* growth trends. Results show the mucin-coated FAMS formulations (e.g., $FAMS_{PGM}$, $FAMS_{BSM}$) supported logarithmic growth of colonizing *E. coli*, with PGM coatings leading to more rapid microbial growth than BSM. Control FAMS prepared with BSA, which serves as a non-mucin protein control ($FAMS_{BSA}$), and the naked material alone (FAMS) showed a significantly blunted growth profile. This suggests that *E. coli* are able to utilize the loaded mucins as a nutrient source to support robust colonization and growth within the coated FAMS materials.

While these results are encouraging, *E. coli* is considered a gastrointestinal pathobiont and so we next tested the canonical probiotic commensals *L. acidophilus* and *L. rhamnosus* (Figure 5g). Visual microscopic inspection of inoculated FAMS gels showed these anaerobic strains more deeply integrated within the synthetic mucus bulk relative to *E. coli*, likely to minimize their exposure to oxygen in solution. Although the media used for these studies contains an L-cysteine reducing agent, the solution is not completely anoxic. As a result, we found that *L. acidophilus* and *L. rhamnosus* were difficult to extract from the entangled fibers during plating assays, leading to an apparent decline in the measured CFU/mL over 24 h (Figure 5g, lower left plots). However, both strains showed a parallel increase in the size of colonies formed on the plated media (Figure 5g, lower right plots), suggesting cohesion of plated bacteria by FAMS fibers. This indicates that the reduction in plated CFU/mL for these strains may be due, in part, to association of the bacteria with the FAMS network, thereby inhibiting its transfer to the agar surface and creating larger seed colonies. Nevertheless, like *E. coli*, both lactobacilli benefit from the presence of mucin-coatings on the FAMS substrate. Finally, to demonstrate that FAMS can support polymicrobial cultures, *E. coli* and *L. rhamnosus* were co-seeded onto BSM-coated materials and bacterial integration visualized via confocal microscopy (Figure 5h–k). After 1 h of incubation, both bacteria were stochastically dispersed throughout the porous material network (Figure 5h), while at 24 h preferential engraftment of both species onto the fibrillar network was observed (Figure 5i). This was particularly noticeable for *L. rhamnosus*, which had a strong preference for adherence to FAMS fibers. This further supports our assertion of lactobacilli entanglement within the FAMS scaffold originally observed during plating studies (Figure 5g). Close inspection of co-inoculated fibrillar bundles showed local interactions of engrafted *E. coli* and *L. rhamosus* colonies (Figure 5j,k). In sum, our results show that gastrointestinal microbiota can successfully integrate into mucin-coated FAMS and colonize the synthetic mucus network to create polymicrobial communities.

Encouraged by these results, we set out to develop a simple, rapid, and low-cost fabrication protocol to generate multilayer microbiome organoids suitable for high throughput screening applications (**Figure 6**a). We began by creating a colorectal epithelial layer using human Caco2 cells cultured for ≥19 days on transwell inserts. Appearance of tight junctions between cells in the monolayer, as indicated by Occludin staining (Figure S9, Supporting Information), confirmed the formation of an organized epithelial interface. We then added the $FAMS_{PGM}$ mucus analog and inoculated with *E. coli* to create the final microbiome model. Orthographic microscopy images shown in Figure 6b demonstrate the 3D layering of each component in the synthetic microbiome. Like native colonic mucosae, FAMS was adhered to the surface of colorectal cells (Figure 6c) and was permeated throughout the

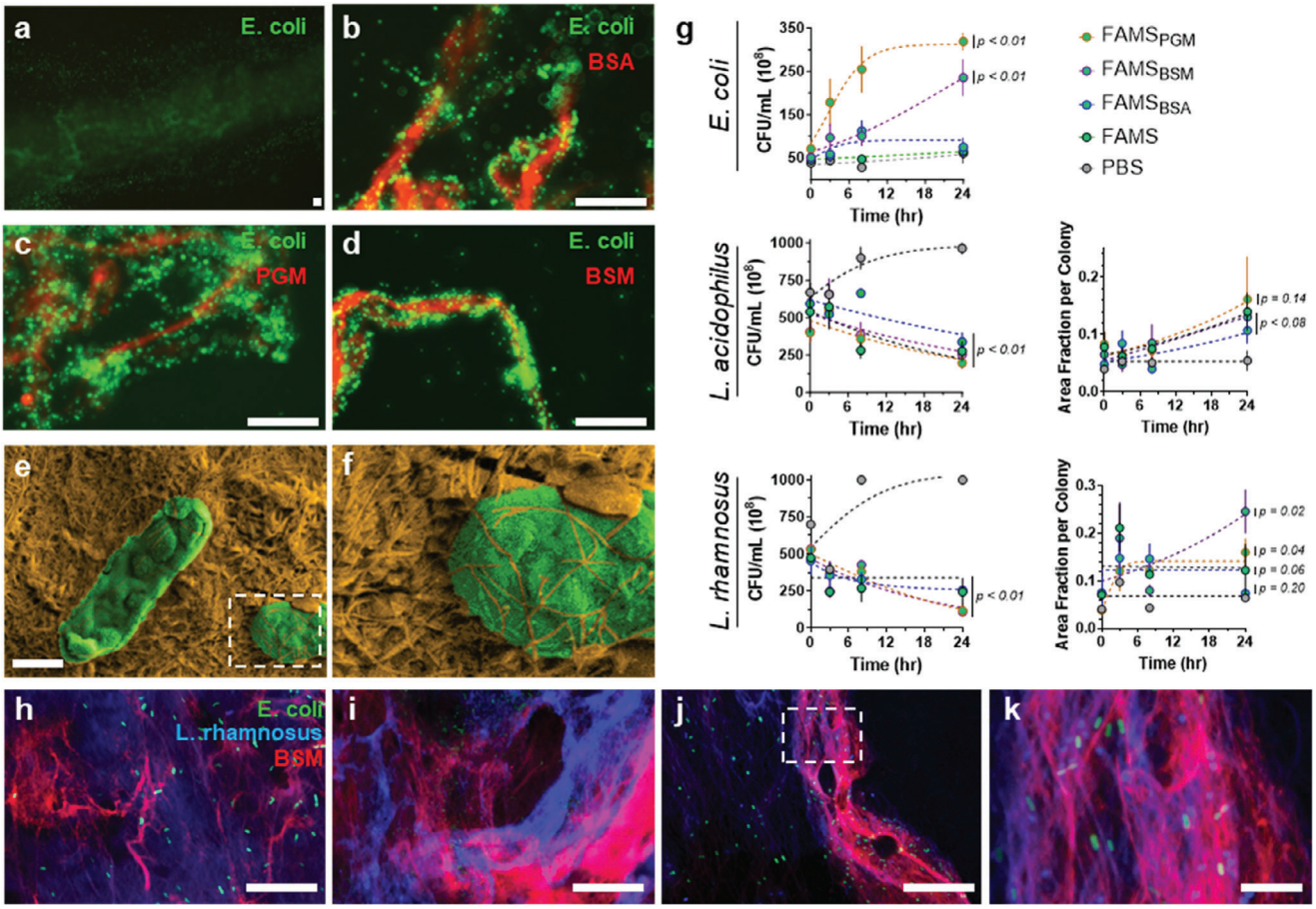

Figure 5. Commensal colonization of FAMS gels. a–d) Representative fluorescent micrographs of GFP-expressing *E. coli* (green) seeded onto uncoated FAMS (a), or b) gels coated with Cy5-labeled (red) BSA, c) PGM, or d) BSM. Scale bars in panel a–d = 500 µm. e) False colored scanning electron micrograph of *E. coli* (green) colonizing FAMS gels (orange). Scale bar = 500 nm. Original, uncolored, images shown in Figure S7 (Supporting Information). f) Magnified region of interest from panel e (dashed white box) demonstrating fibrillar entanglement of colonizing *E. coli* cells. g) Colony formation assays for the indicated gastrointestinal microbe inoculated into blank phosphate buffered saline (PBS, grey) or the indicated FAMS formulation. Plots for *L. acidophilus* and *L. rhamnosus* show time-dependent change in CFU/mL (left) and relative colony size (right). Data shown represents average ± s.e.m. of $n \geq 3$ replicates, with each measure taken from a biological replicate. P values are shown next to the respective formulation and evaluated at the final time point (24 h) relative to PBS control. Replica of panel g with individual data points shown is available in Figure S8 (Supporting Information). h–k) Representative fluorescent confocal micrographs of *E. coli* (green) and *L. rhamnosus* (blue) cultured within BSM-coated FAMS (red) for h) 1 h and i–k) 24 h. Scale bars in panel h–j = 50 µm. k) Magnified region of interest from panel j (dashed white box) demonstrating *E. coli* and *L. rhamnosus* cell-cell and cell-material interactions. Scale bar = 5 µm.

z-plane by colonizing microbes (Figure 6d). Surprisingly, adherence of the Caco2 cell monolayer to FAMS was rapid, leading to sufficient transfer/migration of the cells with/into the fibrillar assembles to remove them from the transwell surface after 1 h of incubation (Figure 6e). Imaging of FAMS-adhered Caco2 cells showed that they remain viable and metabolically active (Figure 6f,g). Although we cannot conclusively rule out some level of Caco2 cell death in these models, our data strongly supports the assertion that Caco2-FAMS-microbe mixtures form a tightly integrated system that reproduces many of the practical structural and morphologic features of native colonic mucus.

The relative ease with which these FAMS-enabled model colonic microbiomes can be constructed highlights their potential for screening applications. As an exemplary demonstration, we tested the permeation of low (4 kDa) and high (70 kDa) molecular weight dextran dyes through the FAMS generated model mucosae (Figure 6h). Permeability assays showed that both the 4 kDa and 70 kDa markers were unable to diffuse across control, unmodified, Caco2 monolayers over the 24-h incubation period (see grey circles in Figure 6h). Conversely, Caco2 monolayers layered with FAMS, either uncoated (FAMS) or functionalized with PGM ($FAMS_{PGM}$), showed an increase in cumulative dextran basolateral diffusion at the 2-h incubation time point, which then generally increased monotonically with time. A slight decline in 4 kDa dextran basolateral fluorescence between the 12- and 24-h measurement time points was observed for the complete Caco2-$FAMS_{PGM}$-*E. coli* mixture (see left plot in Figure 6h). We ascribe this reduction to a metabolism of the dextran dye by *E. coli* at these longer time intervals. Several gastrointestinal bacteria have been reported to metabolize dextran as a nutrient source;[26,27] although we were unable to find a specific reference for the *E. coli* strain used in these assays (101-1). The 70 kDa dextran did

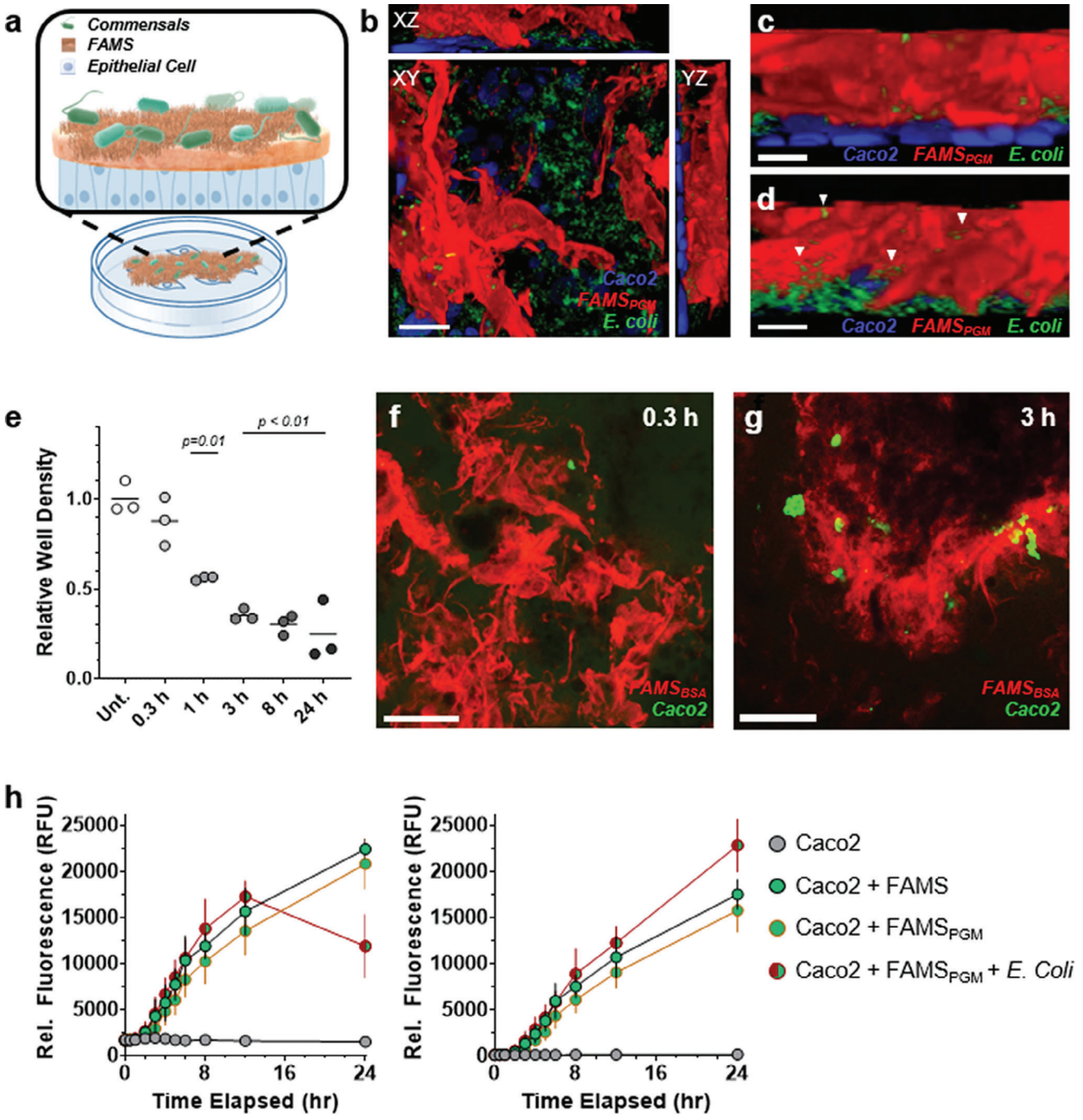

Figure 6. Synthetic microbiome organoids. a) Conceptual schematic of artificial colonic mucosa in a high throughput well plate format. b) Orthographic fluorescent confocal micrographs of synthetic microbiome containing human colorectal Caco2 cells (blue), $FAMS_{PGM}$ (red), and GFP-expressing *E. coli* (green). Scale bar = 20 µm. c,d) Magnified z-stack images of artificial mucosae highlighting FAMS integration with the Caco2 epithelial monolayer (c) and colonization by inoculated *E. coli* ((d) white triangles). Scale bars in panels c and d = 5 µm. e) Relative Caco2 cell density remaining on transwell surface after varying incubation times with $FAMS_{PGM}$. Data shown represents average ± s.e.m. of $n = 3$ replicates. P values for all time points is <0.01 relative to the untreated control (Unt.). f,g) Confocal micrographs of $FAMS_{PGM}$ removed from the surface of Caco2 cell monolayers after f) 0.3 and g) 3 h of incubation. Viable Caco2 cells are stained with calcein-AM (green). Scale bars = 200 µm. h) Time-dependent apical-to-basolateral diffusion of 4 kDa FITC-dextran (left) and 70 kDa rhodamine-dextran (right) across transwell-seeded Caco2 cell monolayers without (grey circle) or with integrated FAMS (green circle), $FAMS_{PGM}$ (green circle/orange border) or $FAMS_{PGM}$ and *E. coli* mixture (green/red circle). Data shown in panel represents average ± s.e.m. of $n = 3$ replicates; panel h represents average ± s.e.m. of $n = 6$ replicates, measured from distinct biological replicates. All confocal micrographs shown are representative images from replicate analyses. Replica of panel h with individual data points shown is available in Figure S10 (Supporting Information).

not show the same decline in fluorescence during the 12–24 h interval, suggesting its higher molecular weight inhibited enzymatic processing.

In vivo pharmacokinetic studies report that 4 kDa dextran permeates the gut and enters systemic circulation as early as 15 min after oral gavage, achieving maximum plasma concentration at 1–4 h; dependent on mouse strain.[28] The same study described slowed gastrointestinal transit kinetics for 70 kDa dextrans compared to 4 kDa markers, with serum bioavailability presumably similarly delayed. Taken in context with our data (Figure 6h), FAMS-generated microbiome organoids appear significantly better at mimicking the in vivo pharmacokinetics of dextran than unfunctionalized Caco2 monolayers, which currently are considered the gold standard for ex vivo drug permeability assays.[29] This is most likely due to mechano-chemical cross-talk between FAMS, *E. Coli* and Caco2 cells, leading to a more permissive mucosal interface that may better replicate the in vivo environment.

3. Outlook

Here, we exploit privileged fluorine-fluorine interactions to template the assembly of a fluorinated amino acid at liquid–liquid phase separated interfaces. The resultant supramolecular matter (fluorine-assisted mucus surrogate, FAMS) is a viscous gel that mimics the double layer architecture of native human colonic mucus. Rheological studies show FAMS resembles the viscoelastic properties of colonic mucus and can be tuned in its mechanical performance via controlling environmental ionic strength and pH. Added mucin proteins rapidly adhere to the surface of the fibrillar network to simulate the proteinaceous profile of mucus without disrupting the viscoelastic properties of FAMS. Together, this generates a colonic mucus surrogate that can be inoculated with gastrointestinal pathobionts or commensals, and added to human colorectal epithelium, to generate a multicellular synthetic microbiome.

It is important to note that the feasibility studies presented here are limited to select model microbiota, and do not yet recapitulate the microorganismal diversity of the human microbiome. Future development of this platform to support engraftment of anaerobic cultures processed from human stool will bring the technology closer to this goal. Nevertheless, we envision these materials will provide a simple, robust, and tractable tool to study commensal biology and microbe-mucus-host interactions ex vivo. The addition of leukocytes may expand this platform to advance our understanding of microbe-immune cell interactions in the gut. Since FAMS utilizes inexpensive and commercially available building blocks, are generated using simple protocols that do not require specialized equipment, and can be integrated with established epithelial models, these materials may have utility in high throughput screening campaigns. As an exemplary application, we show that FAMS can be readily incorporated into standard Caco2-based permeability assays to enhance the prediction of in vivo drug adsorption. Because these FAMS-enabled models can be developed without significant cost or training they represent a complementary alternative to microfluidic and stem cell-based organoid approaches that are currently limited in their broad utility due to complexity and cost.

4. Experimental Section

Materials: Fmoc-pentaflurophenylalanine and thiazolyl blue tetrazolium bromide (MTT) were purchased from Chem Impex. Perfluorodecalin (PFD) and Thioflavin T (ThT) were purchased from Oakwood Chemical. Phosphate buffered saline (PBS, 1x) without calcium and magnesium, Dulbecco's Modified Eagle's Medium (DMEM) with 4.5 g L^{-1} glucose, L-glutamine, and sodium pyruvate, DMEM with 4.5 g L^{-1} glucose and sodium pyruvate, without L-glutamine and phenol red, Falcon 75 cm^2 cell culture flasks, Falcon 1.0 µm pore PET transwell membranes, 96-well tissue culture plates, and Trypan blue 0.4% w/v were purchased from Corning. PBS 10x without calcium and magnesium, bovine serum albumin, LB Miller Broth (granulated), Mueller Hinton Broth 2, bacteriological agar, 6-, 12-, and 24- well tissue culture plates, Nunc Lab-Tek II 4-well chambered coverglass, Prolong Diamond Mountant with DAPI, Gibco 100x Minimum Essential Medium Non-Essential Amino Acids (MEM NEAA), Gibco Trypsin-EDTA 0.25%, Dimethylsulfoxide (DMSO), Slide-a-lyzer 3.5 kDa molecular weight cutoff (MWCO) dialysis cassettes, and adhesive sheets were purchased from Thermo Fisher Scientific. Bovine submaxillary mucin (Type I-S, BSM), mucin from porcine stomach (Type II, PGM), Penicillin-Streptomycin, L-cysteine HCl, Fluorescein isothiocyanate (FITC) Dextran (≈3000–5000 Da), Rhodamine B isothiocyanate Dextran (70 000 Da) were purchased from Sigma Aldrich. Fetal Bovine Serum (FBS) was purchased from VWR. Sulfo-Cy5 NHS ester was purchased from Lumiprobe. Calcein AM was purchased from Cayman Chemical. Rabbit anti-occludin primary antibody and AlexaFluor 488 Goat Anti-Rabbit secondary antibody were purchased from Abcam. Paraformaldehyde (PFA, 4%) was purchased from Santa Cruz Biotechnology. Ampicillin was purchased from Dot Scientific. Difco Lactobacillus MRS broth and Difco Lactobacillus MRS agar were purchased from BD Biosciences.

Caco2 colorectal adenocarcinoma cells, *Lactobacillus acidophilus* (4356), and *Lactobacillus rhamnosus* (9595) were purchased from ATCC. *Escherichia coli* 101-1 was a gift from Dr. Kenneth Keiler at The Pennsylvania State University. Rosetta 2 (DE3) *Escherichia coli* expressing green fluorescent protein (GFP *E. coli*) and recombinantly expressed GFP were gifts from Dr. Joel Schneider at the National Cancer Institute.

FAMS Assembly: Fmoc-F_F was dissolved in room-temperature PFD at 20 mM by vortex mixing, then ultrasonication for 10 min. Fmoc-F_F in PFD solution was added to PBS 1x at 1:10 v:v. This mixture was then emulsified by vortex mixing at 3000 rpm for 1 min. Sealed samples were incubated at 37 °C for 0–72 h before use. Samples for biological and rheological studies were incubated for 48 h before use.

Rheology: Viscoelastic properties of FAMS were measured on a ThermoHaake RotoVisco 1 with cone-and-plate format (L01019C60/1 Ti). BSA, PGM, and BSM were each dissolved to their desired concentration in PBS 1x. Equal volume (2 mL) of each sample was pipetted onto the center of the plate. To avoid disruption of FAMS structure, 2 mL volume samples were constructed in sealed, inverted 24-well microwell plates. The seal was removed to deposit the FAMS sample directly to the center of the plate. Viscosity was measured at constant deformation of 10 Hz for 60 s, capturing data at initiation and once per second thereafter. Each condition was repeated in triplicate ($n = 3$). Dynamic viscosity was calculated by dividing the measured viscosity at each timepoint by the recorded deformation rate.

Fluorescent Spectroscopy and Imaging: Fibrillar assembly was tracked by monitoring ThT binding over several days via fluorescence spectroscopy. Stock ThT solution was created by dissolving powdered ThT in PBS 1x to 2.5 mM. Homogenous ThT solution was added to freshly mixed FAMS to final concentration of 0.05 mM, and samples were incubated at 37 °C for 72 h. ThT activity was tracked by measuring fluorescence across each sample with a Biotek Cytation 3 Imaging Plate Reader. Samples were excited at 430 nm and emission was recorded at 490 nm. Images of fibers with ThT were captured with a Cytation 3 in Brightfield and GFP (excited at 469 nm, detected at 597 nm) channels.

Imaging of protein adsorption to FAMS was performed by first fluorescently labeling BSM, PGM, and BSA with Sulfo-Cy5 NHS Ester. Each protein was dissolved to 5 mg mL^{-1} in 0.1 M $NaHCO_3$ buffer, before addition of Sulfo-Cy5 NHS Ester in 8 molar excess. Protein solution was vortex

mixed with Sulfo-Cy5 NHS solution and kept on ice overnight. Unbound Sulfo-Cy5 NHS Ester was removed by dialysis in 3.5 kDa MWCO cassettes against pure DI water for 24 h. Purified Cy5-tagged protein solutions were frozen at −80 °C overnight, lyophilized to obtain dry powder, and stored at 4 °C until use.

Cy5-tagged proteins were dissolved at 1 mg mL^{-1} in PBS 1x by vortex mixing and 1 h of shaking at 37 °C. Protein solution was added to complete FAMS to achieve final concentration of 0.02 µg mL^{-1} protein in FAMS, then gently mixed. Samples were extracted by pipetting and placed into clean microwell plates for imaging. Fluorescent and brightfield images were captured using a Biotek Cytation 3 in the Texas Red channel (excitation at 586 nm, detection at 647 nm).

Bacterial Growth and FAMS Inoculation: GFP *E. coli* was cultured overnight in LB Miller Broth with 50 µg mL^{-1} ampicillin, shaking at 37 °C. *E. coli* 101-1 was cultured overnight in Mueller Hinton Broth 2, shaking at 37 °C. *L. rhamnosus and L. acidophilus* were cultured overnight in Difco Lactobacillus MRS Broth in stationary capped tubes at 37 °C. Each liquid culture was centrifuged at 6000 x g for 10 min to pellet and resuspended in PBS 1x before use in assays. Growth was assessed by optical density (OD) measurements at 600 nm in polystyrene cuvettes using a ThermoScientific Genesys 150 UV–vis Spectrophotometer. Solution density was normalized to OD = 1.00 in PBS 1x for each bacterial sample to control volume variability in all experiments.

Microbes were cultured in FAMS and supplementary proteins to track survivability. Treatment wells of FAMS were produced in sealed 24-well plates as described above, 1 mL in volume. Wells receiving additional proteins were inoculated with 10 mg mL^{-1} protein solution (PGM, BSM, BSA) to achieve a final concentration of 0.5 mg mL^{-1}. Density-normalized bacterial solution, prepared as above, was used to inoculate each treatment well with final theoretical OD = 0.01. For *E. coli*, no additional supplements were added to the treatment wells. For both *Lactobacillus* species, treatment wells were supplemented with 100 µL Lactobacillus MRS broth and 5 µM L-cysteine to partially reduce the growth environment. Cultures remained in treatment solution for 0–24 h before sampling. Co-culture experiments were conducted under conditions designed for *Lactobacillus* FAMS cultures. Wells were sampled, diluted, and plated onto 50 mm agar plates containing supplement appropriate to the species. For *E. coli* 101-1, plates contained LB Miller broth mixed with bacteriological agar. For both *Lactobacillus* species, plates contained Lactobacillus MRS agar. Dilutions were optimized for each species to facilitate colony forming unit (CFU) counting assays. After 24–48 h of incubation, each plate was photographed. ImageJ was used to analyze the images to obtain a metric of CFU/mL for each sample.

Electron Microscopy: Scanning electron microscopy (SEM) was accomplished by drying samples (20 µL) of FAMS, protein-coated FAMS, and *E. coli* – loaded FAMS on 12.7 mm Aluminum specimen mounts (Ted Pella, Inc., 6 mm Pin, Zeiss). Samples were gold-palladium coated using a Bal-tec SCD-050 sputter coater. Micrographs were obtained using a Zeiss VP-FESEM with electron high tension of 3.5 kV and working distance 3.3–5.3 mm. Facilities used for SEM were courtesy of the Huck Institutes of Life Sciences Microscopy Facility at The Pennsylvania State University. Images were false colored in Adobe Photoshop where indicated.

Confocal Imaging of Synthetic Microbiome Organoids: Models of synthetic microbiome organoids were made using FAMS, colorectal cancer cells, fluorescently-tagged mucins, and fluorescent bacteria. Colorectal cancer cells (Caco2) were seeded onto 4-well chambered cover glass at 1.5×10^5 cells cm^{-2}. Culture media was DMEM with 4 mM L-glutamine, 10% FBS, Penicillin-Streptomycin (100 units and 0.1 mg mL^{-1}, respectively), and 1x MEM NEAA. Cells were cultured to 80% confluence, changing media every 4 days. Cell monolayer was fixed with 4% PFA for 15 min, washed twice with PBS 1x, then nuclei were stained with Hoechst 33 342 (5 µg mL^{-1}). After 20 min, cells were washed twice with PBS 1x. Pre-made FAMS was added to the chamber wells by pipetting. Cy5-PGM was added in solution to achieve final concentration of 0.5 mg mL^{-1} in the chamber wells. Density-normalized solution of GFP *E. coli* was added to chamber wells to a theoretical OD = 0.01. Synthetic microbiome organoids were imaged using a Zeiss LSM 880 Airyscan Fast at the Huck Institutes of Life Sciences Microscopy Facility at The Pennsylvania State University. Images were captured in three channels using Zeiss Zen Black microscopy software: Hoechst 33 342 (excited at 405 nm, detected between 410 and 483 nm), EGFP (excited at 488 nm, detected between 493 and 597 nm), and Cy5 (excited at 633 nm, detected between 638 and 759 nm).

Transmembrane Diffusion: Colorectal cancer cells (Caco2) were seeded onto 1.0 µm pore PET transwell membranes in 6-well plates at 1.5×10^5 cells cm^{-2}. Cells were cultured 19–23 days until immunostaining for occludin via application of rabbit anti-occludin primary antibody for 30 min at 1 µg mL^{-1}, followed by Alexa Fluor 488 Goat Anti-Rabbit IgG H&L for 30 min at 7.5 µg mL^{-1}. Transwell membranes were cut from the membrane chamber using a surgical blade. The membranes were fixed to glass slides with ProLong Diamond Mountant with DAPI and covered with #1 glass covers. Slides were imaged by confocal microscopy with a Zeiss LSM 880, with excitation at 488 nm and detection at 495–630 nm. After satisfactory tight junction formation had been achieved, media was removed and 2 mL FAMS material including PGM (0.5 mg mL^{-1}) and 101-1 *E. coli* (theoretical OD = 0.01) was added in the apical chamber. The basolateral chamber was filled with 3 mL phenol red-free DMEM as formulated above. FITC-labeled (≈3000–5000 g mol^{-1}) and Rhodamine B-labeled (70 000 g mol^{-1}) dextrans were added to achieve 5 µM concentration of each in the apical chamber. Sample volumes were collected from the basolateral chambers of each transwell assembly over 24 h. Plates were kept at 37 °C, 5% CO2 between samplings. Plates containing *E. coli* were kept in an independent incubator at similar conditions. Diffusion was measured by fluorescence of the basolateral media samples, in both FITC (excitation 488 nm, detection 525 nm) and Rhodamine B (excitation 586 nm, 647 nm).

Cell Detachment: Caco2 monolayers were cultured on transwell membranes as described above. After incubation with FAMS at varying timepoints, transwells were washed with three times with PBS 1x. MTT solution was added to each well to achieve final concentration of 0.5 mg mL^{-1}, then incubated at 37 °C for 3 h. MTT solution was removed and replaced with 100% DMSO, then MTT crystals were dissolved by shaking for 15 min at room temperature. Absorbance was measured across the area of each well at 570 nm using a Biotek Cytation 3.

To assess cell attachment/migration onto/into FAMS, Caco2 cells were cultured similarly in 12-well plates. At 80% confluence, cells were treated with FAMS and Cy5-BSA (0.5 mg mL^{-1}), then incubated at 37 °C, varying duration. Wells were then treated with Calcein AM (5 µM final conc.) for 30 min. Samples for imaging were extracted by pipetting the supernatant FAMS from each well into a clean 12-well plate. Samples were imaged by confocal microscopy with a Zeiss LSM 880, exciting at 488 nm for Calcein AM (detected 493–616 nm) and 633 nm for Cy5-BSA (detected 638–759 nm).

Statistical Analyses: Experiments are represented as a mean of independent replicates, with standard error of the mean (s.e.m.) where indicated in the figure caption. Data was analyzed using GraphPad Prism 9 software. P values, where shown, are indicators of significance obtained from unpaired Student's t-tests using equal variance.

Supporting Information

Supporting Information is available from the Wiley Online Library or from the author.

Acknowledgements

Confocal microscopy and scanning electron microscopy were performed at the Penn State Microscopy and Cytometry Facility, University Park, PA. The authors would like to thank Dr. Atip Lawanprasert for assistance with electron microscopy and Dr. Cheng Dong for assistance with viscometry rheological studies. Funding for this work was provided by NSF DMR-1845053 and NIH 1R35-GM142902 to S.M. Funds from the Penn State University Graduate Fellowship supported M.A.M.

Conflict of Interest

The authors declare no conflict of interest.

Data Availability Statement

The data that support the findings of this study are available from the corresponding author upon reasonable request.

Keywords

fluorine, interface, microbiome, mucus, self-assembly

Received: February 8, 2024
Published online: March 13, 2024

[1] R. E. Ley, D. A. Peterson, J. I. Gordon, *Cell* **2006**, *124*, 837.
[2] M. Arumugam, J. Raes, E. Pelletier, D. Le Paslier, T. Yamada, D. R. Mende, G. R. Fernandes, J. Tap, T. Bruls, J.-M. Batto, M. Bertalan, N. Borruel, F. Casellas, L. Fernandez, L. Gautier, T. Hansen, M. Hattori, T. Hayashi, M. Kleerebezem, K. Kurokawa, M. Leclerc, F. Levenez, C. Manichanh, H. B. Nielsen, T. Nielsen, N. Pons, J. Poulain, J. Qin, T. Sicheritz-Ponten, S. Tims, et al., *Nature* **2011**, *473*, 174.
[3] A. B. Shreiner, J. Y. Kao, V. B. Young, *Curr. Opin. Gastroenterol.* **2015**, *31*, 69.
[4] M. H. Mohajeri, R. J. M. Brummer, R. A. Rastall, R. K. Weersma, H. J. M. Harmsen, M. Faas, M. Eggersdorfer, *Eur. J. Nutr.* **2018**, *57*, 1.
[5] J. Halfvarson, C. J. Brislawn, R. Lamendella, Y. Vázquez-Baeza, W. A. Walters, L. M. Bramer, M. D'Amato, F. Bonfiglio, D. McDonald, A. Gonzalez, E. E. McClure, M. F. Dunklebarger, R. Knight, J. K. Jansson, *Nat. Microbiol.* **2017**, *2*, 17004.
[6] C. M. Guinane, P. D. Cotter, *Ther. Adv. Gastroenterol.* **2013**, *6*, 295.
[7] B. A. Helmink, M. W. Khan, A. Hermann, V. Gopalakrishnan, J. A. Wargo, *Nat. Med.* **2019**, *25*, 377.
[8] M. H. Mohajeri, G. La Fata, R. E. Steinert, P. Weber, *Nutr. Rev.* **2018**, *76*, 481.
[9] J. F. Cryan, S. O'mahony, *Neurogastroenterol. Motil.* **2011**, *23*, 187.
[10] J. W. Arnold, J. Roach, A.-P. MA, *Trends Microbiol.* **2016**, *24*, 887.
[11] R. U. Sheth, V. Cabral, S. P. Chen, H. H. Wang, *Trends Genet.* **2016**, *32*, 189.
[12] A. D. Kostic, M. R. Howitt, W. S. Garrett, *Genes Dev.* **2013**, *27*, 701.
[13] M. Poletti, K. Arnauts, M. Ferrante, T. Korcsmaros, *J. Crohns. Colitis.* **2021**, *15*, 1222.
[14] S. Bartfeld, *Dev. Biol.* **2016**, *420*, 262.
[15] M. Biancalana, S. Koide, *Biochim. Biophys. Acta - Proteins Proteomics* **2010**, *1804*, 1405.
[16] D. M. Ryan, T. M. Doran, S. B. Anderson, B. L. Nilsson, *Langmuir* **2011**, *27*, 4029.
[17] J. N. Sloand, T. E. Culp, N. M. Wonderling, E. D. Gomez, S. H. Medina, *Adv. Funct. Mater.* **2021**, *31*, 2104223.
[18] J. P. Celli, B. S. Turner, N. H. Afdhal, S. Keates, I. Ghiran, C. P. Kelly, R. H. Ewoldt, G. H. McKinley, P. So, S. Erramilli, R. Bansil, *Proc. Natl. Acad. Sci.* **2009**, *106*, 14321.
[19] S. Cornick, A. Tawiah, K. Chadee, *Tissue Barriers* **2015**, *3*, e982426.
[20] P. Paone, P. D. Cani, *Gut* **2020**, *69*, 2232.
[21] R. L. Howard, M. Markovetz, Y. Wang, C. Ehre, S. Z. Sheikh, N. L. Allbritton, D. B. Hill, *Biophys. J.* **2021**, *120*, 5384.
[22] D. Larobina, A. Pommella, A.-M. Philippe, M. Y. Nagazi, L. Cipelletti, *Proc. Natl. Acad. Sci.* **2021**, *118*, e2103995118.
[23] S. K. Lai, Y.-Y. Wang, D. Wirtz, J. Hanes, *Adv. Drug Delivery Rev.* **2009**, *61*, 86.
[24] Y. Guo, Y. Ma, X. Chen, M. Li, X. Ma, G. Cheng, C. Xue, Y. Y. Zuo, B. Sun, *ACS Nano* **2023**, *17*, 2813.
[25] A. Rajbhandary, B. L. Nilsson, *Pept. Sci.* **2017**, *108*, e22994.
[26] G. R. Gibson, A. Willems, S. Reading, M. D. Collins, *Proc. Nutr. Soc.* **1996**, *55*, 899.
[27] E. Khalikova, P. Susi, T. Korpela, *Microbiol. Mol. Biol. Rev.* **2005**, *69*, 306.
[28] A. Woting, M. Blaut, *Nutrients* **2018**, *10*, 685.
[29] I. Hubatsch, E. G. Ragnarsson, P. Artursson, *Nat. Protoc.* **2007**, *2*, 2111.